# Pleiotropic Phenotypes of the *sticky peel* Mutant Provide New Insight into the Role of *CUTIN DEFICIENT2* in Epidermal Cell Function in Tomato[1][W][OA]

**Satya Swathi Nadakuduti, Mike Pollard, Dylan K. Kosma, Charles Allen Jr., John B. Ohlrogge, and Cornelius S. Barry***

Department of Horticulture (S.S.N., C.A., C.S.B.) and Department of Plant Biology (M.P., D.K.K., J.B.O.), Michigan State University, East Lansing, Michigan 48824

Plant epidermal cells have evolved specialist functions associated with adaptation to stress. These include the synthesis and deposition of specialized metabolites such as waxes and cutin together with flavonoids and anthocyanins, which have important roles in providing a barrier to water loss and protection against UV radiation, respectively. Characterization of the *sticky peel* (*pe*) mutant of tomato (*Solanum lycopersicum*) revealed several phenotypes indicative of a defect in epidermal cell function, including reduced anthocyanin accumulation, a lower density of glandular trichomes, and an associated reduction in trichome-derived terpenes. In addition, *pe* mutant fruit are glossy and peels have increased elasticity due to a severe reduction in cutin biosynthesis and altered wax deposition. Leaves of the *pe* mutant are also cutin deficient and the epicuticular waxes contain a lower proportion of long-chain alkanes. Direct measurements of transpiration, together with chlorophyll-leaching assays, indicate increased cuticular permeability of *pe* leaves. Genetic mapping revealed that the *pe* locus represents a new allele of *CUTIN DEFICIENT2* (*CD2*), a member of the class IV homeodomain-leucine zipper gene family, previously only associated with cutin deficiency in tomato fruit. *CD2* is preferentially expressed in epidermal cells of tomato stems and is a homolog of Arabidopsis (*Arabidopsis thaliana*) *ANTHOCYANINLESS2* (*ANL2*). Analysis of cuticle composition in leaves of *anl2* revealed that cutin accumulates to approximately 60% of the levels observed in wild-type Arabidopsis. Together, these data provide new insight into the role of *CD2* and *ANL2* in regulating diverse metabolic pathways and in particular, those associated with epidermal cells.

Plants are continually exposed to environmental changes that impact their fitness and survival. Changes in light intensity, light quality, temperature, and water availability occur on a daily basis and insect pests and pathogens pose a constant threat. Consequently, plants have evolved a suite of physical and chemical adaptations and defenses against abiotic and biotic stresses that have facilitated their colonization of diverse environments. The surface properties of plants are crucial to their successful adaptation to stress. The epidermal cell layer and associated structural appendages such as trichomes, together with the cuticle form the primary physical and chemical barriers that protect plants against multiple stresses (Glover, 2000; Sieber et al., 2000; Schilmiller et al., 2008; Javelle et al., 2011b). Furthermore, the surface properties of plants are dynamic and can change in response to stress, therefore influencing the physiology of the plant (Lu et al., 1996; Ingram et al., 2000; Abe et al., 2003; Ingram, 2008; Kosma et al., 2009; Wang et al., 2011).

The metabolism of epidermal cells is programmed for the synthesis of lipids that form the cuticle, a heterogeneous lipid-based barrier comprised of cutin, intra, and epicuticular waxes and polysaccharides that covers the aerial surfaces of all terrestrial plants. In addition to serving as the principal barrier to water loss (Kolattukudy, 1980; Riederer and Schreiber, 2001; Pollard et al., 2008) the cuticle provides structural support, possesses antiadhesive properties that limit pathogen infection, resists insect feeding and oviposition, and has reflective properties that reduce heat load and limit the effect of UV radiation (Bargel et al., 2006). Furthermore, the chemical properties of the cuticle are dynamic with both cuticle deposition and wax composition altering in response to water stress and abscisic acid (Kosma et al., 2009; Wang et al., 2011). The epidermal and subepidermal cells are also sites of phenylpropanoid biosynthesis, and in particular the synthesis and accumulation of flavonoids and anthocyanins (Martin and Gerats, 1993; Hichri et al., 2011; Matas et al., 2011). Anthocyanins protect plants through

[1] This work was supported by Michigan State University AgBioResearch, a Strategic Partnership Grant from the Michigan State University Foundation, the National Science Foundation (grant nos. IOS–1025636 [to C.S.B.] and MCB–0615563 [to J.B.O. and M.P.]), and the Department of Energy Great Lakes Bioenergy Research Center (Department of Energy Office of Science Biological and Environmental Research DE–FC02–07ER64494). C.A. was supported by the Plant Genomics@MSU internship program.

* Corresponding author; e-mail barrycs@msu.edu.

The author responsible for distribution of materials integral to the findings presented in this article in accordance with the policy described in the Instructions for Authors (www.plantphysiol.org) is: Cornelius S. Barry (barrycs@msu.edu).

[W] The online version of this article contains Web-only data.

[OA] Open Access articles can be viewed online without a subscription.

www.plantphysiol.org/cgi/doi/10.1104/pp.112.198374

their UV radiation absorbing properties and their synthesis is influenced by stress and can vary with light intensity and wavelength (Beggs et al., 1987; Li et al., 1993; Christie et al., 1994; Landry et al., 1995; Fuglevand et al., 1996; Steyn et al., 2002). Together, these studies highlight the importance of the epidermal cell layer in the synthesis of compounds important for stress adaptation in plants that likely contributed to colonization of the terrestrial environment by early land plants (Edwards et al., 1996; Cooper-Driver, 2001).

Many enzymes, transporters, and regulatory factors required for the biosynthesis and deposition of cuticular lipids have been identified and characterized in Arabidopsis (*Arabidopsis thaliana*; Li et al., 2007, 2010a; Panikashvili et al., 2007, 2009; Samuels et al., 2008; Li-Beisson et al., 2010; McFarlane et al., 2010; Seo et al., 2011; Wu et al., 2011). Tomato (*Solanum lycopersicum*) fruit also serve as a powerful system for investigating the physical properties and biosynthesis of the cuticle fostered in large part by the abundance of cuticular lipid deposited during fleshy fruit development, its astomatous nature, and relevance in fruit cracking and postharvest storage (Emmons and Scott, 1997, 1998; Matas et al., 2004; Bargel and Neinhuis, 2005). Genomics- and proteomics-based approaches have identified genes and proteins preferentially expressed in the fruit peel, and perturbation of several genes through mutagenesis has revealed altered fruit cuticle phenotypes (Vogg et al., 2004; Hovav et al., 2007; Mintz-Oron et al., 2008; Isaacson et al., 2009; Yeats et al., 2010; Matas et al., 2011).

Fruit of the *sticky peel* (*pe*) mutant of tomato have a rubbery surface texture rather than the typical smooth surface associated with wild-type fruit, rendering fruits sticky to the touch (Butler, 1952). In addition, *pe* fruits have a highly glossy fruit surface, a phenotype recently associated with cutin deficiency (Isaacson et al., 2009). In this study, a combination of microscopy and chemical analysis revealed that *pe* fruit are cutin deficient and have an altered wax profile. In addition, several phenotypes attributed to altered epidermal cell function are apparent in *pe*, including cutin deficiency and altered wax deposition in leaves, together with increased cuticular permeability, lower trichome density, and reduced anthocyanin accumulation. Genetic mapping indicated that *pe* encodes a new allele of *CUTIN DEFICIENT2* (*CD2*), which encodes a member of the class IV homeodomain-Leu zipper (HD-ZIP IV) family, and was previously only associated with a fruit-specific reduction in cuticle biosynthesis (Isaacson et al., 2009). In addition, we show that mutation in a *CD2* homolog at the *anthocyaninless2* (*anl2*) locus of Arabidopsis also causes a cutin-deficient phenotype in rosette leaves. Together, these data identify additional roles for *CD2* and *ANL2*, defining a regulatory link between cuticle and flavonoid biosynthesis, two pathways that operate within epidermal cells that are critical for plant responses to stress.

## RESULTS

### Introgression of the *pe* Allele into the Ailsa Craig Genetic Background

At the initiation of this research, the genetic background of the *pe* mutant was unknown. Therefore, we initiated a backcross strategy to introgress the *pe* mutation into the Ailsa Craig (AC) genetic background, a cultivar previously selected for introgression of varied morphological mutants of tomato (Darby et al., 1978). The mutant and wild-type plants used in the following experiments were derived from a $BC_3F_2$ population that we estimate contains approximately 93.75% of the AC genetic background. Therefore, the influence of the genetic background on the data presented is likely to be minimal.

### Altered Morphology and Trichome Chemistry of the *pe* Mutant

In addition to the previously documented sticky peel phenotype of *pe* fruit (Butler, 1952), the *pe* mutant exhibits a short stature with pale-green leaves and stems (Fig. 1A). Five-week-old wild-type AC plants had an average dry weight of 6.45 g whereas the dry weight of *pe* plants was 3.86 g. Glandular trichomes are epidermal cell appendages that are prevalent on the surface of tomato plants and synthesize a suite of specialized metabolites known, or hypothesized to play a role in plant defense responses against pests and pathogens (Schilmiller et al., 2008). Type VI glandular trichomes are the most abundant glandular trichomes on the tomato leaf surface (Kang et al., 2010) and these are reduced greater than 3-fold in *pe* (Fig. 1, B–D). The type VI glandular trichomes of cultivated tomato synthesize a mixture of mono- and sesquiterpenes of which $\beta$-phellandrene predominates (Schilmiller et al., 2009). The volatile terpene levels in leaf dips of AC and *pe* were compared (Supplemental Fig. S1). Consistent with the reduced abundance of type VI glandular trichomes on the surface of *pe* leaves, volatile terpene levels are also significantly reduced to approximately 16% of that observed in wild type.

### Reduced Anthocyanin Accumulation in *pe*

To investigate the pale phenotype of *pe* in more detail, chlorophyll and anthocyanin levels were determined in fully expanded and meristematic leaves. Chlorophyll levels in AC and *pe* are not significantly altered but anthocyanin content is reduced by approximately 85% in *pe* (Table I). The anthocyanins represent an end point of the phenylpropanoid pathway and are known to accumulate in epidermal and subepidermal cell layers (Martin and Gerats, 1993; Hichri et al., 2011). The distribution of anthocyanins within the stems of AC and *pe* was compared by confocal laser-scanning microscopy and stems of the *high pigment-1* (*hp-1*) and *entirely anthocyaninless* (*ae*) mutants were included as positive and negative controls,

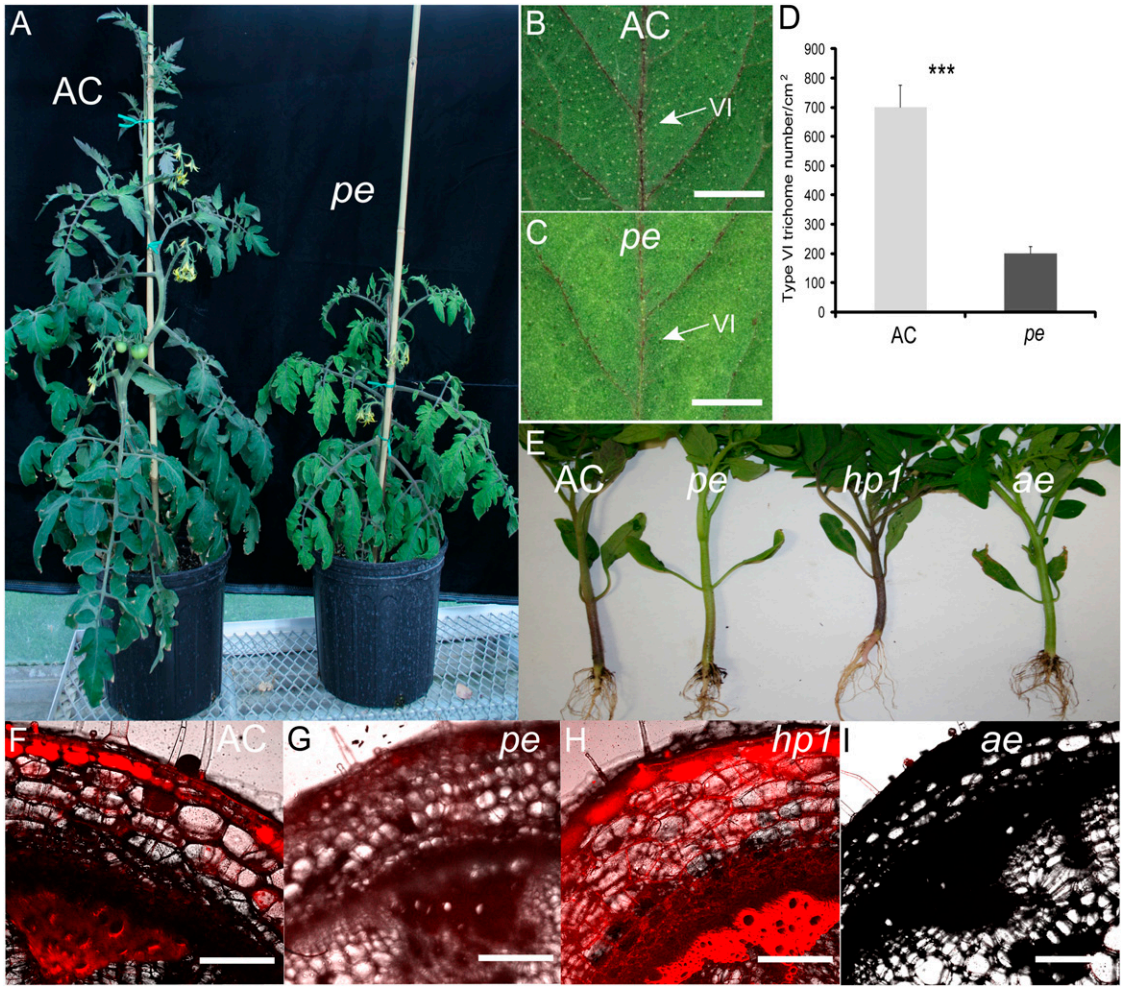


**Figure 1.** Phenotypic variation between AC and *pe*. A, Whole-plant phenotype of AC and *pe*. B and C, Light micrographs of trichomes on leaves of AC and *pe*. Type VI glandular trichomes are indicated by arrowheads, scale bar = 2 mm. D, Density of glandular type VI trichomes on the adaxial leaf surface of AC and *pe*. Data are presented as the mean of $n = 8 \pm$ SE on adaxial side of AC and *pe* leaves. Asterisks denote significant differences (***, $P < 0.001$) as determined by Student's *t* tests. E, Comparison of anthocyanin accumulation in the stems of AC and *pe*. Stems of the *hp1* and *ae* mutants are shown for comparison. F to I, Autofluorescence of anthocyanins in AC, *pe*, *hp1*, and *ae* visualized by confocal laser-scanning microscopy (scale bar = 200 $\mu$m).

respectively (Fig. 1, E–I). Images reveal two main patterns of anthocyanin distribution in AC, with accumulation observed in the epidermal and subepidermal cells and also surrounding the vasculature (Fig. 1F). In contrast anthocyanin accumulation is greatly reduced in stems of *pe* (Fig. 1G).

### Lignin Content Is Not Altered in *pe*

Like anthocyanins, lignin also represents an end point of the phenylpropanoid pathway (Vogt, 2010). Reduced lignin synthesis in plants is associated with stunted growth, mediated by increased salicylic acid levels (Brown et al., 2001; Li et al., 2010b; Gallego-Giraldo et al., 2011). To investigate whether the semidwarf phenotype of *pe* is related to reduced accumulation of lignin, the total lignin content in leaves and stems of AC and *pe* was analyzed. The total percent acetyl bromide soluble lignin (% ABSL) as well as individual lignin monomers of AC and *pe* leaves showed no significant differences between the two genotypes (Supplemental Table S1).

### The *pe* Fruit Cuticle Has Altered Physical and Chemical Properties

Fruits of the *pe* mutant are highly glossy and are sticky to the touch when compared to wild type (Fig. 2, A and B; Butler, 1952). In addition, we observed that ripe *pe* fruits are generally crack resistant. The average Young's elastic modulus (Y) is approximately 2-fold greater than wild type, indicating increased stiffness of the *pe* fruit peel (Fig. 2C). Glossiness and increased

**Table I.** *Anthocyanin and chlorophyll content of AC and pe leaves*

Data represent the mean of $n = 5 \pm$ SE. Asterisks denote significant differences between genotypes of the same developmental stage (***, $P < 0.001$) as determined by Student's *t* tests.

| Compound | Mature Leaves | | Meristematic Leaves | |
|---|---|---|---|---|
| | AC | *pe* | AC | *pe* |
| Anthocyanin content (AU 535 nm $g^{-1}$ FW) | 12.4 ± 2.1*** | 1.9 ± 0.6 | 13.1 ± 1.0*** | 5.4 ± 0.63 |
| Chlorophyll content ($\mu g\ mL^{-1}$) | 54.8 ± 2.0 | 53.3 ± 3.1 | 67.3 ± 0.6 | 66.4 ± 0.8 |

stiffness in tomato fruit peels is associated with cutin deficiency (Isaacson et al., 2009). Scanning electron microscopy (SEM) images of *pe* fruit indicated reduced cuticle deposition compared to AC fruit (Fig. 2, D–G). Staining of cryosections of the fruit peel of AC and *pe* with the lipid reactive stain, Sudan IV confirmed reduced cuticle lipid deposition in the *pe* mutant (Fig. 2, H and I).

The chemical composition of *pe* fruit cuticles is significantly altered compared to that of AC fruits. The cutin monomer load (mass/area) in ripe *pe* fruits is approximately 2% of that in AC and 6.5% of AC levels in green fruits (Table II). Furthermore, the large reduction in cutin monomer content is observed for all hexadecanoic-acid-derived cutin monomers, together with cis- and trans-coumaric acid, products of the phenylpropanoid pathway. The notable exception to the general reduction of cutin monomers in *pe* is the abundance of the hexadecanoic acid itself, which has slightly increased abundance in mutant fruit, particularly at the green stage of development.

Altered glossiness of plant surfaces is often associated with changes in wax composition (Chen et al., 2003; Aharoni et al., 2004; Bourdenx et al., 2011). The total wax load is not significantly different between AC and *pe* fruits at either the green or ripe stages of development (Supplemental Table S2). However, the cutin monomer to wax ratio, signifying relative proportion of wax within the cutin matrix, falls dramatically from approximately 75:1 (1,086.5:14.42 $\mu g\ cm^{-2}$) in ripe fruits of AC to 1.6:1 (26.1:15.7 $\mu g\ cm^{-2}$) in *pe* (Table II; Supplemental Table S2). Also, the composition of individual wax components is significantly altered. For example, alkanes constitute approximately 40% of the total wax load in AC fruits but between 55% and 62% in *pe* fruits due largely to increases in C31 to C33 alkanes at both the green and ripe stages of fruit development (Fig. 3; Supplemental Tables S2 and S3). Fatty acids constitute a relatively minor component of the total wax load ranging from 2% to 5% in both AC and *pe* and there are no significant differences at the green stage, although ripe fruits of the mutant have a significantly higher fatty acid content due mainly to a 2-fold increase in hexadecanoic acid. In contrast to the general increase in the levels of long-chain alkanes and fatty acids in the epicuticular wax of *pe*, the fatty alcohols (alkanols and alkenols) together with coumarates, sterols, and triterpenoids show a general reduction in *pe* compared to AC. In particular, the amyrins, which accumulate to similar levels as the alkanes in wild-type fruit, are reduced by approximately 86% in green fruit of *pe* (Fig. 3; Supplemental Tables S2 and S3). Alkanes are well known to constitute much of the epicuticular wax, whereas triterpenoids are almost exclusively intracuticular waxes (Vogg et al., 2004). Thus the reduction in triterpenoids but not alkanes with the loss of cutin is consistent with the differential localization of these waxes.

### Altered Surface Chemistry and Increased Water Conductance in *pe* Leaves

To investigate whether the altered surface chemistry observed in *pe* is restricted to fruit or is a more general phenotype of the mutant, the cutin and wax composition of the leaves of AC and *pe* were compared. As was observed in fruit, the major monomer identified in tomato leaf cutin is also 9(10),16-dihydroxyhexadecanoic acid, constituting between 20% and 25% of the total cutin monomer load (Fig. 4). Additional monomers identified include several fatty acids and the phenylpropanoids cis- and trans-coumaric acid together with caffeic acid. The overall cutin monomer load in leaves of *pe* is 54% of that in AC, with an approximately 5-fold reduction in 9(10), 16-dihydroxyhexadecanoic acid and significant reductions in additional monomers (Fig. 4A).

Tomato leaf cuticular wax components identified in this study comprise *n*-alkanes, isoalkanes, anteiso alkanes, petacyclic triterpenoids, sterol derivatives, and fatty acids. Among these, alkanes and branched alkanes constituted the major fraction (up to 90%) of all the identified wax composition in wild-type leaves. The total leaf wax load is reduced by 30% in the mutant. This is mainly attributed to significant reduction in alkanes. Interestingly all the straight-chain alkanes in the *pe* mutant were reduced by approximately 50% compared to wild type, whereas branched-chain alkanes are essentially unaltered (Fig. 4B). As both wax and cutin loads decrease in leaf, unlike in fruit (Table II; Supplemental Table S2), the cutin monomer to wax ratio changes only fractionally in the *pe* mutant, from 2.3 (5.85:2.53 $\mu g\ cm^{-2}$) to 1.8 (3.20:1.80 $\mu g\ cm^{-2}$; Fig. 4). This clearly shows a differential regulation of straight-chain and branched hydrocarbons in fruit and leaf cuticular wax, suggesting they may be independently regulated.

Cuticular waxes play a pivotal role in limiting water loss in plants. The levels of alkanes within cuticular waxes are often positively correlated with increased

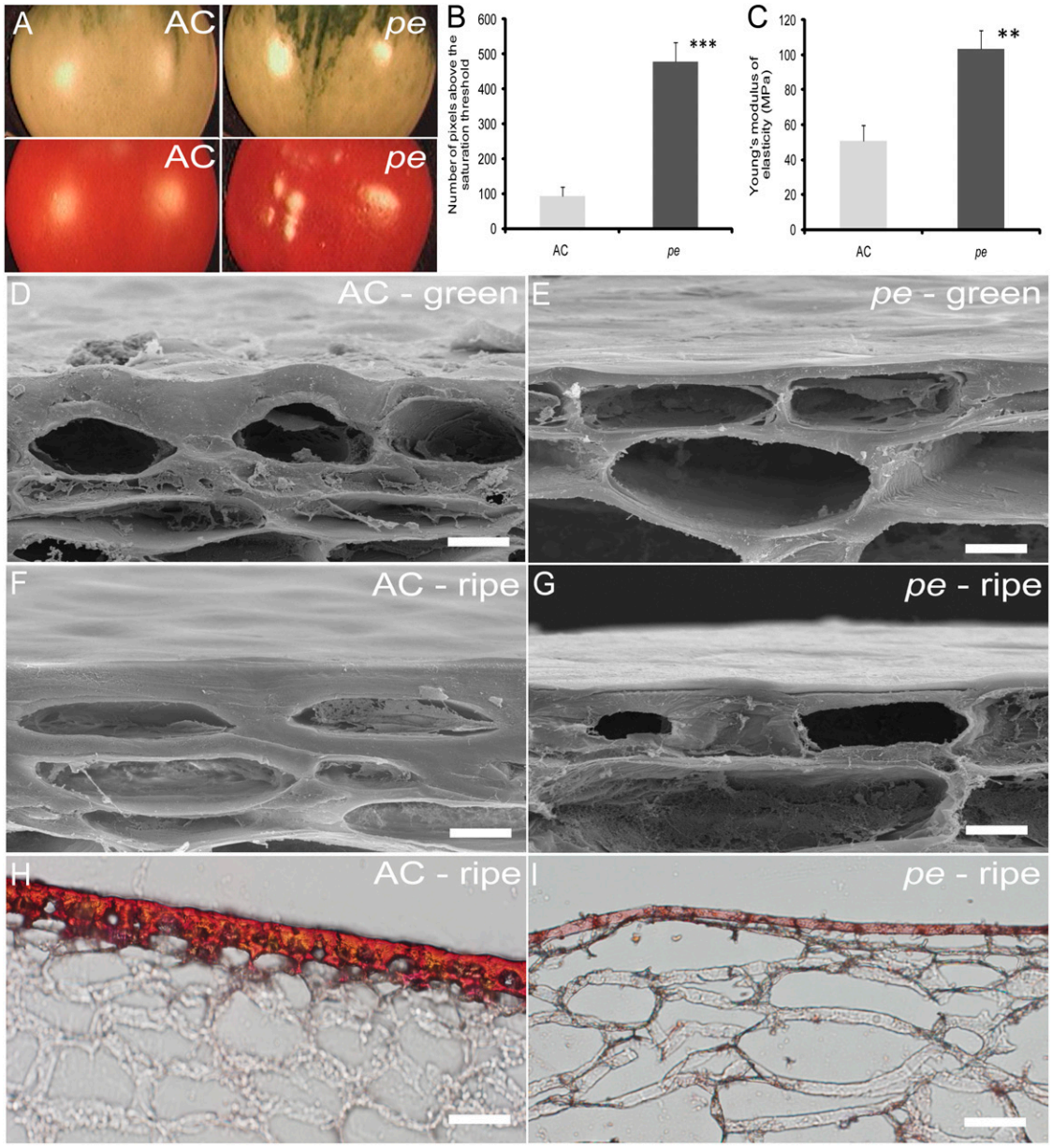


**Figure 2.** Fruit phenotypes of *pe*. A, Increased glossiness in *pe* fruits compared to AC. B, Quantitative analysis of glossiness in ripe fruits of AC and *pe*. The values of number of pixels above the saturation threshold represent the mean values ($n = 5$) ± SE. C, Average Young's modulus of elasticity ($n = 5$) ± SE. Asterisks denote significant differences (**, $P < 0.01$; ***, $P < 0.001$) as determined by Student's *t* tests. D to G, Scanning electron micrographs of AC and *pe* fruits at the green and ripe stages of development. Note reduced cuticle deposition in the *pe* mutant (scale bar = 20 $\mu$m). H and I, Light micrographs of cuticular lipid distribution in ripe fruits using Sudan IV staining. Scale bar = 50 $\mu$m.

resistance to cuticular water loss and an increase in cuticular wax abundance, particularly alkanes can occur during water stress (Grncarevic and Radler, 1967; Kosma et al., 2009; Bourdenx et al., 2011; Seo et al., 2011). Furthermore, altered cutin composition may disrupt the intermolecular packing of waxes within the cutin matrix, although this relationship remains unclear (Pollard et al., 2008; Schreiber, 2010; Buschhaus and Jetter, 2011). Given the reduction in alkane and cutin monomer content in the leaves of the *pe* mutant, the rate of leaf water loss from mutant leaves was determined. The *pe* mutant does not have an obviously wilty phenotype however leaf water conductance in intact *pe* leaves was approximately 3-fold higher than in AC (Fig. 5A). Similarly, an increase in the rate of chlorophyll leaching was observed in *pe* leaves (Fig. 5B), a phenomena previously shown to be associated with cuticle permeability (Kosma et al., 2009). Previous research indicated that defects in cutin biosynthesis can lead to alterations in stomatal structure including

**Table II.** *Cutin monomer composition in fruit cuticles of AC and pe in μg cm$^{-2}$ (%)*

Data represent the mean of $n = 5 \pm$ SE. Asterisks denote significant differences between genotypes of the same developmental stage (*, $P < 0.05$; ***, $P < 0.001$) as determined by Student's *t* tests. ND, Not detected.

| Cutin Monomer | Green Fruit | | Ripe Fruit | |
|---|---|---|---|---|
| | AC | *pe* | AC | *pe* |
| cis-coumarate | 4.8 ± 1.1 (1.6) | ND | 6.9 ± 0.8 (0.6) | ND |
| trans-coumarate | 11.3 ± 2.5 (3.6)*** | 0.6 ± 0.1 (2.9) | 27.6 ± 3.4 (2.5)*** | 0.5 ± 0.1 (2.0) |
| Hexadecanoic acid | 0.7 ± 0.1 (0.2) | 1.82 ± 0.6 (9.0)* | 1.3 ± 0.2 (0.1) | 1.4 ± 0.7 (5.4) |
| Hexadecane 1,16-dioic acid | 6.2 ± 1.0 (2.0) | ND | 12.7 ± 1.7 (1.2)*** | 0.4 ± 0.1 (1.7) |
| C16:1 hexadecenoic acid | 1.6 ± 0.1 (0.5) | ND | 9.3 ± 1.3 (0.9)*** | 0.2 ± 0.05 (0.8) |
| 16-OH hexadecanoic acid | 4.7 ± 1.1 (1.5)*** | 0.32 ± 0.05 (1.6) | 22.6 ± 3.9 (2.1)*** | 0.4 ± 0.1 (1.6) |
| 9-OH, 16-oxo hexadecanoic acid | 3.9 ± 0.4 (1.3) | ND | 25.2 ± 5.0 (2.3)*** | 0.4 ± 0.1 (1.5) |
| Octadecane 1,16-dioic acid | 2.1 ± 0.2 (0.7) | ND | 3.8 ± 0.6 (0.4) | ND |
| 8-OH hexadecane 1,16-dioic acid | 2.5 ± 0.4 (0.8) | ND | 18.3 ± 4.3 (1.7)*** | 0.6 ± 0.1 (2.1) |
| 18-OH octadecanoic acid | 2.3 ± 0.6 (0.7) | ND | 7.8 ± 1.2 (0.7)*** | 0.3 ± 0.1 (1.2) |
| 10, 16-diOH hexadecanoic acid | 176.4 ± 6.0 (57.1)*** | 3.1 ± 1.4 (15.5) | 827.2 ± 18.5 (76.1)*** | 6.8 ± 0.9 (26.0) |
| 9, 18-diOH octadecanoic acid | 2.2 ± 0.6 (0.7) | ND | 12.6 ± 1.9 (1.2)*** | 0.1 ± 0.05 (0.4) |
| Unidentified | 90.0 ± 19.3 (29.2) | 14.4 ± 1.2 (71.0) | 111.2 ± 20.5 (10.2) | 14.9 ± 4.4 (57.1) |
| Total | 308.8 ± 20.5*** | 20.2 ± 1.2 | 1086.5 ± 22.1*** | 26.1 ± 5.9 |

impaired development of cuticular ledges that lie between adjacent guard cells (Li et al., 2007). Scanning electron micrographs of the leaf surface did not reveal any structural differences in the stomata of the *pe* mutant (Fig. 5C). Furthermore, the average stomatal density on the abaxial leaf surface in wild-type leaves (30 in 0.55 mm$^2$) is higher than in *pe* leaves (21 in 0.55 mm$^2$; Fig. 5D). Together, these data suggest that enhanced rate of water loss from the leaves of *pe* mutant is due to cuticular water loss and not to altered stomatal structure or density.

### Root Suberin and Wax Composition Are Not Dramatically Altered in *pe*

The altered cutin and wax composition observed in the leaves and fruits of *pe* suggested the possibility of a general perturbation in synthesis of fatty-acid-derived polymers. This was investigated by determining the suberin and wax content in roots of *pe*. The aliphatic components that account for nearly 90% of the total suberin, together with the aromatic components are not significantly altered in *pe* (Supplemental Fig. S2A). In addition, the overall root wax load is largely unaltered in *pe* although small increases in abundance of β-C22:0 monoacyl-glycerol, C29:2 sterol, and C18:0 and C22:0 primary alcohols are observed (Supplemental Fig. S2B).

### Mapping of the *pe* Locus and Candidate Gene Identification

The *pe* locus was provisionally mapped to chromosome 1 of the classical genetic map of tomato (Mutschler et al., 1987). An F2 mapping population segregating for the *pe* mutant allele was generated through crosses between tomato (*pe*/*pe*; LA2467) and *Solanum pimpinellifolium* (*PE*/*PE*; LA1589). The mutant plants were pale green in color and this phenotype cosegregated with the cutin-deficient, sticky and glossy fruit phenotype in the F2 population. The F2 population was genotyped with chromosome 1 molecular markers, revealing that the *pe* locus is located within a 424-kb interval

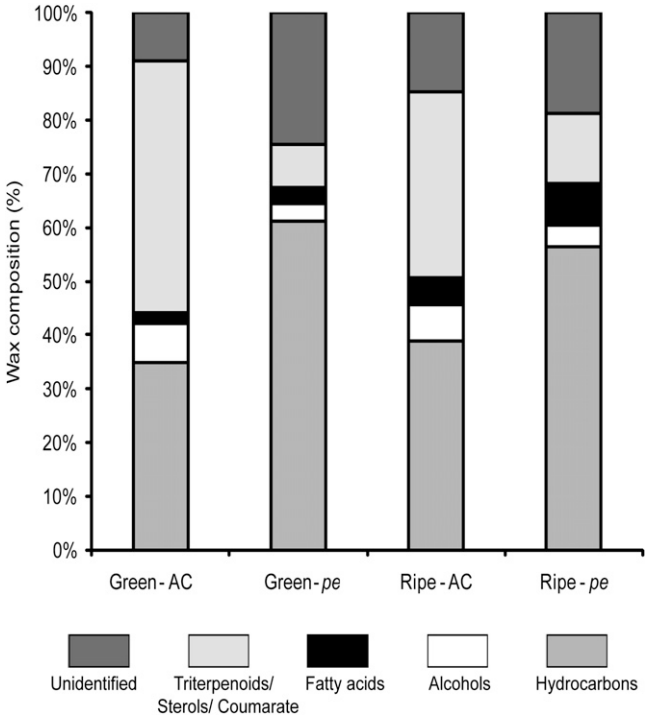


**Figure 3.** Relative fruit wax composition in AC and *pe*. Fruit wax content of green and ripe stage fruits were analyzed by GC. The wax components were grouped under five classes; (1) hydrocarbons, consisting of alkanes, branched alkanes and alkenes, (2) alcohols, (3) fatty acids, (4) triterpenoids, sterols, and coumarates, and (5) unidentified compounds. The relative percentage of each class comprising the total wax load is shown.

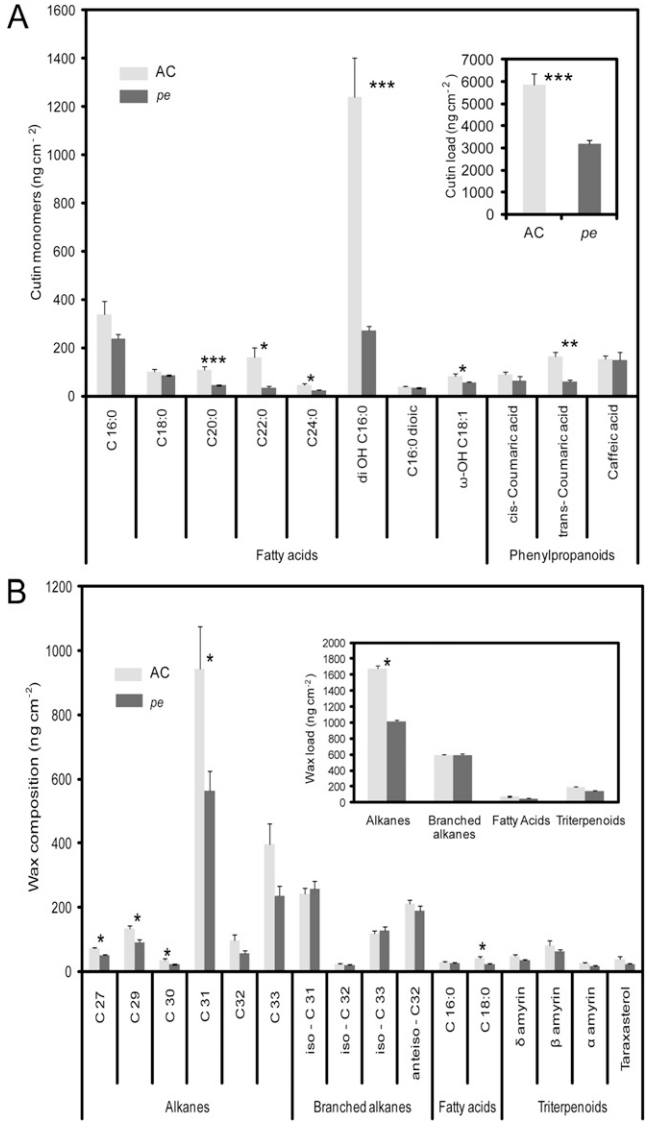


**Figure 4.** Leaf cutin and wax profiles of AC and *pe*. A, Leaf cutin components were grouped into (1) fatty acids and (2) phenylpropanoids. B, Leaf wax constituents were grouped into four classes; (1) alkanes, (2) branched chain alkanes, (3) fatty acids, and (4) triterpenoids. Inset graphs indicate total cutin and wax loads in AC and *pe*. Values represent mean values ($n = 5$) ± SE. Asterisks denote significant differences (*, $P < 0.05$; **, $P < 0.01$; ***, $P < 0.001$) as determined by Student's *t* tests.

between C2_At4g00090 and cTOA-13-J3 (Fig. 6A). This mapping interval contains the *CD2* gene, which encodes a HD-ZIP IV protein, with homology to *ANL2* of Arabidopsis (Kubo et al., 1999; Isaacson et al., 2009). A single G > A substitution causes the conversion of a conserved Gly to Arg at position 736 of the protein at the *cd2* locus that results in a glossy and cutin-deficient fruit phenotype with a total cutin load of approximately 10% of wild-type fruits (Isaacson et al., 2009). The similarity in phenotype and map position of *pe* and *cd2* suggested that *pe* may be allelic to *cd2*. To investigate this hypothesis, the *CD2* gene was cloned and sequenced from the *pe* mutant, revealing the insertion of a G nucleotide following nucleotide 2045. This insertion causes a frame-shift mutation, resulting in the incorporation of four spurious amino acids followed by a premature stop codon that truncates the predicted protein by 160 amino acids in *pe* (Fig. 6A).

To confirm that a mutation in the *CD2* gene is responsible for the *pe* mutant phenotype, virus-induced gene silencing (VIGS) experiments were performed using two constructs targeting separate regions of the *CD2* gene. *CD2*-silenced lines showed a 20% to 30% reduction in height compared with TRV2 empty vector control lines and leaves showed sectors of pale coloration characteristic of the *pe* mutant (Fig. 6, B–D). Anthocyanin levels were reduced in the *CD2*-silenced lines by approximately 30% to 35% (Fig. 6E). The major leaf cutin monomer 9 (10),16-dihydroxyhexadecanoic acid was reduced by 50% in the silenced lines and there was a concomitant increase in the leaf water conductance (Fig. 6, F and G). Together, these data indicate that the *pe* mutant phenotype is caused by a mutation in *CD2*.

### Mutation at the *anl2* Locus Leads to Cutin Deficiency

Phylogenetic analysis indicated that CD2 is closely related to a number of HD-ZIP IV proteins including several that impact epidermal cell development and cuticle biosynthesis (Nakamura et al., 2006; Javelle et al., 2010, 2011a; Fig. 7A). *HD-ZIP IV* genes are typically expressed in epidermal cells and expression analysis indicated that *CD2* transcripts are enriched in stem peels, which are comprised of a mixture of epidermal and subepidermal cells, compared to the levels observed in whole stem and stem core with the peel removed (Fig. 7B).

*ANL2* is the closest Arabidopsis homolog to *CD2* (Fig. 7A) and is also preferentially expressed in epidermal cells (http://efp.ucr.edu/cgi-bin/absolute.cgi). Furthermore, both *pe* and *anl2* mutants have reduced anthocyanin accumulation (Kubo et al., 1999; Fig. 1). These similarities led us to hypothesize that *anl2* mutants would also be cutin deficient. This was confirmed in rosette leaves of *anl2*, which exhibit approximately a 40% reduction in cutin monomer load together with a 25% reduction in the alkane load of the cuticular waxes compared to Columbia-0 (Fig. 8).

## DISCUSSION

### Characterization of *pe* Identifies Additional Roles for *CD2*

Phenotypic characterization indicates that the *pe* mutant has altered fruit surface chemistry, leading to reduced cutin levels and a modified surface wax composition (Fig. 2; Table II; Supplemental Table S2). The altered chemical profile leads to a change in the physical properties of the fruit peel including increased

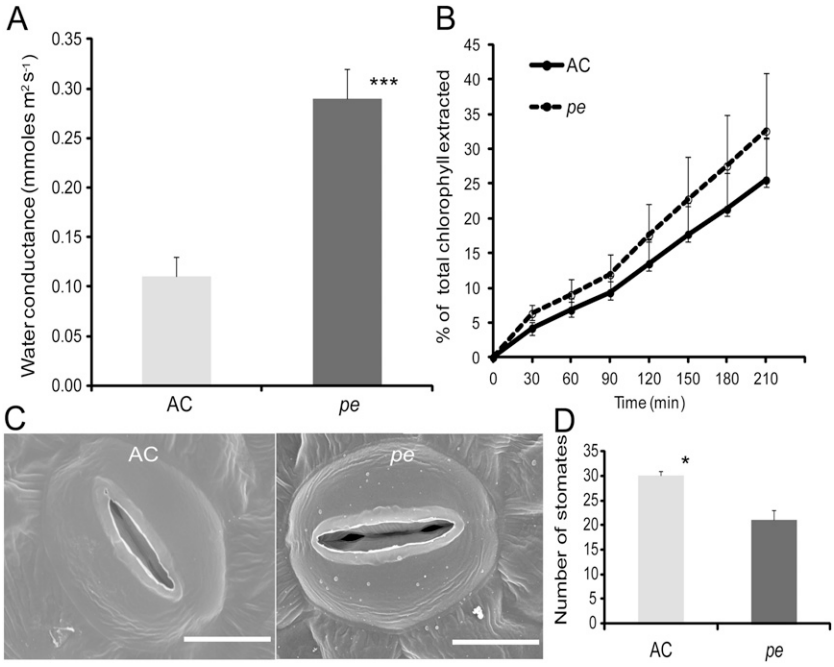


**Figure 5.** Increased cuticular permeability in *pe*. A, Leaf water conductance in AC and *pe* ($n = 5$) ± SE. B, Chlorophyll leaching expressed as percent of total leaf chlorophyll extracted after 24 h ($n = 5$) ± SE. C, Scanning electron micrographs of representative stomata on the abaxial leaf surface of AC and *pe* (scale bar = 5 $\mu$m). D, Stomatal density on abaxial leaf surface area of 0.55 mm$^2$ ($n = 10$ ± SE). Asterisks denote significant differences (*, $P < 0.05$; ***, $P < 0.001$) as determined by Student's *t* tests.

glossiness and a higher Young's elastic modulus (Fig. 2, A–C). These phenotypes are identical to those previously described in *cd* mutants of tomato where cutin deficiency was correlated with altered biomechanical and structural properties together with enhanced susceptibility to microbial infection (Isaacson et al., 2009). A combination of genetic mapping and gene cloning revealed that *pe* represents a new mutant allele of *CD2* that truncates the predicted protein by 160 amino acids and therefore likely represents a null allele (Fig. 6A).

Previously, the *cd2* phenotype was associated with fruit-specific alteration in cuticle biosynthesis (Isaacson et al., 2009). However, as shown in this study, many additional phenotypes are evident in *pe* including a semidwarf stature, reduced anthocyanin accumulation, altered cutin and wax deposition in leaves, increased permeability of the leaf cuticle, and reduced trichome density together with lower volatile terpene production (Figs. 1, 4, and 5; Table I; Supplemental Fig. S1). These phenotypes were confirmed in the *cd2* allele and VIGS lines targeting *CD2* (Fig. 6; Supplemental Figs. S3 and S4). Together, these data reveal a broad role for *CD2* in plant development, and particularly in relation to metabolism within epidermal and subepidermal cells, which is supported by the epidermal enriched expression pattern of *CD2* in stems (Fig. 7B) and in tomato fruit (Matas et al., 2011).

### HD-ZIP IV Proteins and Cuticle Biosynthesis

*CD2* belongs to a subgroup of HD-ZIP IV proteins, several of which have defined roles in epidermal cell development and are preferentially expressed within the epidermis (Fig. 7B; Javelle et al., 2011a). Proteins of this family are characterized by HD-ZIP domain followed by a steroidogenic acute regulatory lipid transfer domain. The fact that HD-ZIP IV proteins are widely distributed in lower plants, gymnosperms, and angiosperms but are absent in algae is consistent with a role in the evolution of land plants (Ponting and Aravind, 1999; Mukherjee et al., 2009). Several closely related *CD2* homologs influence cuticle composition and/or regulate genes involved cuticle biosynthesis. For example, *OUTER CELL LAYER1* (*OCL1*) of maize (*Zea mays*) is expressed early in embryo development, prior to protoderm formation and is subsequently expressed in the L1 cell layer in the shoot apical meristem (Ingram et al., 1999). Overexpression of *OCL1* in maize altered the wax composition in leaf blade as well as sheath and increased the expression of several genes involved in wax biosynthesis and transport (Javelle et al., 2010). Furthermore, transient assays suggested that activation of the expression of a wax transporter and a nonspecific lipid-binding protein likely occurs through direct binding of OCL1 to regulatory regions within these genes (Javelle et al., 2010). Similarly, Arabidopsis *HDG1* directly regulates the expression of *BODYGUARD* and *FIDDLEHEAD*, two genes involved in cuticle biosynthesis and disruption of *HDG1* function leads to cuticles with increased permeability (Wu et al., 2011). Furthermore, Arabidopsis *ANL2* and *HDG1* are preferentially expressed in epidermal or subepidermal cells (Suh et al., 2005; Kubo et al., 2008; http://efp.ucr.edu/cgi-bin/absolute.cgi) and our analysis indicates that *anl2* has a cutin-deficient phenotype (Fig. 8).

Overall, the characterized members of the *CD2* subclade all possess a common role in the regulation of cuticle biosynthesis, even though the composition of cutin can vary between species and tissues. For

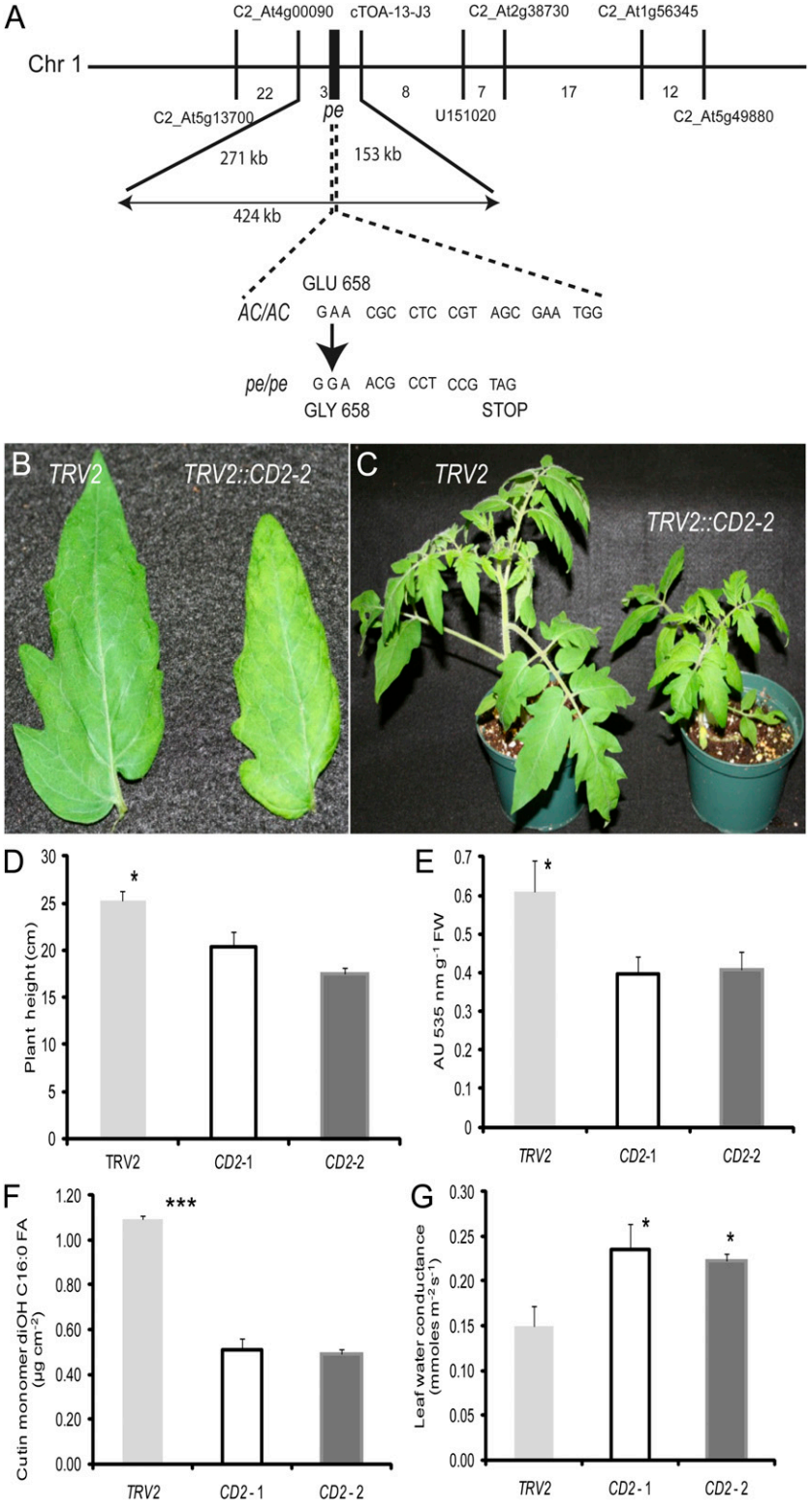


**Figure 6.** Characterization of the *pe* locus and silencing of *CD2*. A, Genetic map of the *pe* locus. Genetic markers and the number of recombinant individuals between adjacent markers from a total of 114 F2 plants are shown. The approximate physical distance between the flanking markers and the *pe* locus is indicated. Sequence analysis of the *CD2* gene from AC and *pe* revealed a single G nucleotide insertion following nucleotide 2045, leading to a frame-shift mutation. B to G, Silencing of *CD2* recreates the *pe* mutant phenotype. B, Pale-leaf phenotype in a *CD2-2* VIGS line. C, Short stature of a *CD2-2* VIGS line. D, Plant height of *CD2* VIGS lines. E, Anthocyanin content of *CD2* VIGS lines. F, The major leaf cutin monomer 9(10),16-dihydroxyhexadecanoic acid is reduced in *CD2*-silenced lines. G, *CD2* silencing impairs leaf cuticle barrier properties and increases water conductivity. All values in D to G, represent mean values ($n = 5$) ± SE. *TRV2* empty vector control lines were used for all comparisons. Asterisks denote significant differences (*, $P < 0.05$; ***, $P < 0.001$) as determined by Student's *t* tests.

example, while tomato cutin is predominantly comprised of hexadecanoic-acid-derived monomers, Arabidopsis leaves have a C18:2 dicarboxylic-acid-rich cutin (Table II; Figs. 4 and 8). These cutins require different sets of biosynthetic genes (Li et al., 2007; Pollard et al., 2008; Li-Beisson et al., 2009), suggesting that while the regulation of cuticle biosynthesis may be generally conserved, these regulatory proteins may target distinct sets of biosynthetic genes in diverse species or tissues contributing to their different cuticle

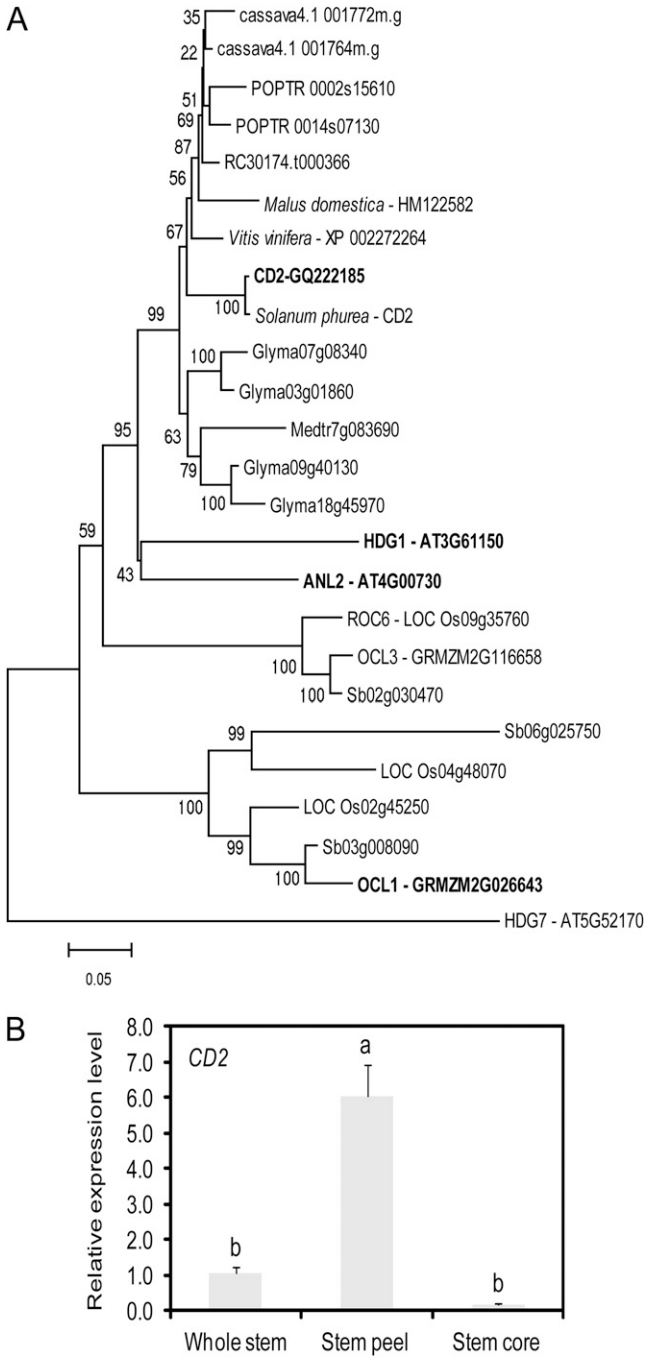


**Figure 7.** Phylogenetic and expression analysis of *CD2*. A, A neighbor-joining phylogenetic tree derived from a multiple sequence alignment of the deduced full-length amino acid sequences of CD2 homologs constructed using MEGA V5.0 software (Tamura et al., 2011). *HDG7* is included as an outgroup. Bootstrap values are from 2,000 replicates, indicated above the nodes. Proteins highlighted in bold have defined functions in cuticle biosynthesis. B, Quantitative reverse transcription PCR analysis of *CD2* expression in stem peel of AC relative to stem core and whole stem. Three biological and three technical replications for each sample were analyzed. Data are presented as the mean expression values ± SE relative to that observed in whole stem. Values labeled with different letters are significantly different (least square means, $P < 0.05$).

composition. Furthermore, given that several members of the *CD2* subclade influence cuticle biosynthesis (Fig. 7A), it is possible that the phylogenetically closely related and as-yet-uncharacterized genes, may also have a similar role.

### A Role for *CD2* in Reducing Leaf Water Loss

The cuticle regulates nonstomatal water loss and the amount and composition of cuticular wax is associated with cuticle permeability to water. For example, mutants or transgenic lines with reduced levels of very-long-chain alkanes often display elevated rates of water loss (Vogg et al., 2004; Leide et al., 2007; Qin et al., 2011). Furthermore, enhancing the levels of these wax components can restrict water loss, leading to improved drought tolerance (Bourdenx et al., 2011; Seo et al.,

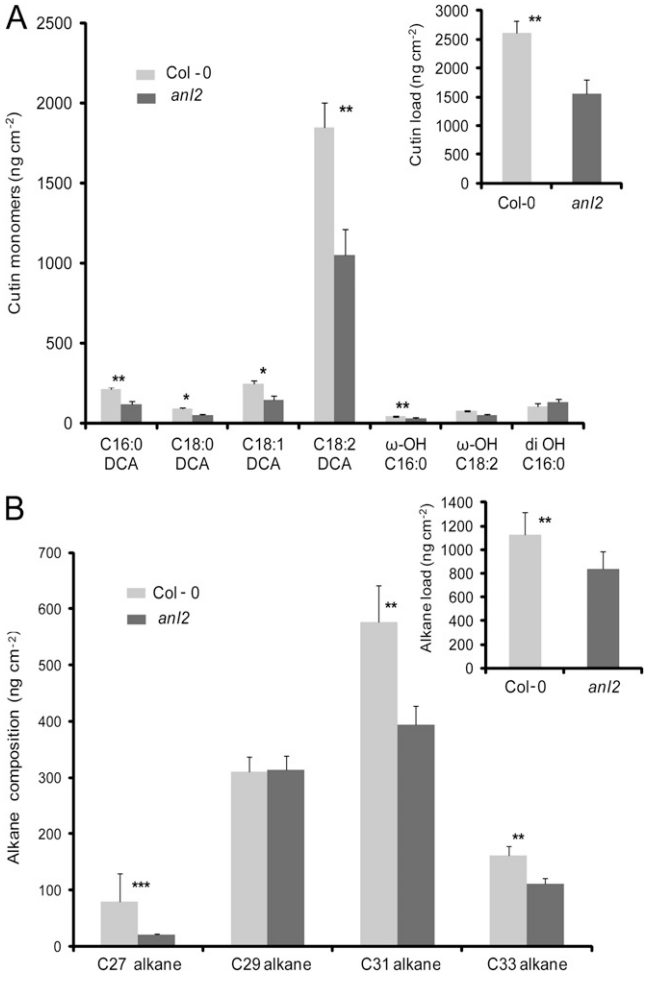


**Figure 8.** Cutin monomer and wax profile of Arabidopsis Columbia-0 and *anl2* leaves. A, Leaf cutin monomer composition ($\alpha$, $\omega$ dicarboxylic acids [DCA]). B, Alkane constituents of leaf wax. Inset graphs indicate total cutin and alkane load. Data represent mean values ($n = 5$) ± SE. Asterisks denote significant differences (*, $P < 0.05$; **, $P < 0.01$; ***, $P < 0.001$) as determined by Student's $t$ tests.

2011). Similarly, drought-stressed plants can increase cuticular wax biosynthesis as a defense mechanism to reduce further water loss (Kosma et al., 2009).

The wax composition of leaves and fruits vary in *pe* when compared to AC. For example, hydrocarbons are elevated in *pe* fruits whereas in leaves the straight-chain alkanes are significantly reduced compared to wild type (Fig. 4B; Supplemental Table S3). The same trend for cutin and wax is observed in the fruit (Isaacson et al., 2009) and leaves (Supplemental Fig. S3) of *cd2* when compared to the M82 parental line. The basis for the differential *CD2*-mediated control of wax accumulation in leaves and fruits is currently unclear but may occur through altered gene regulation between these tissues or possibly altered fluxes of precursors in mutant tissues. For example, a proportion of the hexadecanoic acid precursor, typically utilized in cutin biosynthesis may be channeled toward alkane biosynthesis when cuticle biosynthesis is limited in *pe* and *cd2* fruits. However, this is unlikely to be a general phenomenon as an increase in alkane accumulation is not observed in *cd1* and *cd3* fruits (Isaacson et al., 2009).

Our data suggest a correlation between cuticular wax composition in *pe* and leaf cuticle permeability. For example, leaf water conductance and chlorophyll leaching are increased in *pe* leaves compared to AC (Fig. 5). A similar trend was observed in *CD2*-silenced lines (Fig. 6G). In contrast, fruits of the *pe* and *cd2* mutants, which have higher levels of long-chain alkanes, do not exhibit enhanced rates of postharvest water loss (Supplemental Table S3; Isaacson et al., 2009). Although disruption of individual cutin or wax components can alter permeability, the physical consequences of these changes on the structure of the cutin matrix, is not well understood. Alkanes are proposed to influence cuticle permeability by forming water-impermeable crystalline regions within the cuticle and the packaging of the wax crystals is likely dependent upon the cutin structure (Pollard et al., 2008; Buschhaus and Jetter, 2011). Therefore, while it is not possible to more exactly define the underlying reason for the increased permeability of *pe* leaves, it could be due to one, or a combination of the following factors, including decreased alkane levels, a decreased cutin load, an alteration in the cutin to wax ratio, or an as-yet-undefined biochemical change. A comparison of wax biosynthesis between wild-type and *pe* leaves and fruit tissues, together with a more in-depth understanding of wax deposition in these genotypes and tissues, may provide insight into how *CD2* influences cuticular permeability.

Leaf water loss is also intricately linked to stomatal structure and physiology and several lines of research have highlighted possible links between cuticle composition and stomatal density and structure. Cutin deficiency in Arabidopsis leads to altered stomatal morphology including a reduction in the cuticular ledges (Li et al., 2007). No structural alterations were observed in stomata of the *pe* mutant, suggesting that *CD2* may not influence cuticle biosynthesis in leaf guard cells (Fig. 5C). Similarly, previous reports have shown that altered cuticular wax composition can positively or negatively influence stomatal density in Arabidopsis (Gray et al., 2000; Chen et al., 2003; Yang et al., 2011). The exact mechanisms through which this process occurs are unknown although it is possible that the altered composition of leaf cuticular waxes in *pe* may exert a compensatory influence, leading to the observed reduction in stomatal density (Fig. 5D).

### *CD2* and Phenylpropanoid Biosynthesis

Flux into the phenylpropanoid pathway through the enzyme Phe ammonia lyase represents a branch point between primary and specialized metabolism in plants. The phenylpropanoid pathway synthesizes a wide range of compounds including flavonols, anthocyanins, lignins, suberin and cutin aromatics, and tannins, which have diverse roles in plants as structural polymers, pigments, UV protectants, and signaling molecules (Hahlbrock and Scheel, 1989; Vogt, 2010). In agreement with the epidermal enriched expression pattern of *CD2* (Fig. 7B), the *pe* mutant exhibits reduced accumulation of a subset of phenylpropanoids that typically are synthesized and accumulate in the epidermal and subepidermal cells. In addition to the anthocyanins that are severely reduced in *pe* tissues, coumarates, which comprise between 3% and 5% of the total cutin monomer load in wild-type tomato fruits, are also reduced in *pe* (Fig. 1; Tables I and II). The reduction in coumarate is readily ascribed to the reduction of the cutin aliphatic hydroxy fatty acid monomers, to which coumarate is likely esterified. In contrast, the abundance of lignin and suberin ferulates, two biopolymers derived from phenylpropanoid precursors that are not typically associated with epidermal cells, are unaltered in *pe* (Supplemental Fig. S2; Supplemental Table S1). It will be of interest to determine if additional phenylpropanoid-derived metabolites are altered in the epidermal cells of *pe* and to understand the flux through the pathway in these cells in the *pe* mutant. In addition, the role of *CD2*/*ANL2* in directly regulating anthocyanin biosynthesis, as well as understanding their relationship to known transcriptional regulators of anthocyanin biosynthesis warrants additional investigation.

### *CD2* as a Regulator of Epidermal Cell Function

HD-ZIP IV proteins are master regulators of epidermal cell fate and function in higher plants and have roles in cuticle biosynthesis together with patterning of trichome and stomata (Javelle et al., 2011a). Our biochemical characterization of the *pe* mutant of tomato has revealed alterations in multiple pathways associated with epidermal cell function that have evolved to facilitate plant adaptation to stress, including altered cuticle biosynthesis in leaves and fruits,

reduced anthocyanin accumulation, and lower trichome and stomatal densities. The subsequent identification of *pe* as an allele of *CD2* extends current knowledge of the role of *CD2* beyond cuticle biosynthesis in tomato fruit to include a spectrum of altered phenotypes associated with epidermal cell function. While mutant alleles of *CD2* influence a broad range of epidermal cell phenotypes, it is difficult to determine whether these alterations constitute primary or secondary effects. For example, altered stomatal and trichome densities can result from perturbation of cuticular wax biosynthesis, including mutations that affect catalytic enzymes, suggesting that disruption of cuticle structure and/or physiology induces secondary phenotypes (Gray et al., 2000; Chen et al., 2003; Kurata et al., 2003; Aharoni et al., 2004). Establishing cause and effect relationships with respect to the altered stomatal and trichome density phenotypes observed in *pe* will be complex.

Our data suggest that *CD2* is a master regulator of epidermal cell function in tomato. Although the exact role of *CD2* in specifying epidermis-related phenotypes remains to be defined, it is possible that CD2 directly regulates the expression of the biosynthetic genes involved in synthesis of diverse epidermal cell associated molecules. Alternatively, it is equally probable that CD2 acts upstream of these pathways, within a transcriptional network that maintains epidermal cell identity and function. Defining the immediate targets of CD2 will provide insight into these questions and will help identify the regulatory networks that control specialized metabolism within plant epidermal cells.

## MATERIALS AND METHODS

### Plant Material and Growth Conditions

Seeds of the *pe* (*pe/pe*; LA2467), *hp-1* (*hp-1/hp-1*; LA3538), and *ae* (*ae/ae*; LA3612) mutants, together with *Solanum pimpinellifolium* (LA1589) were obtained from the Tomato Genetics Resource Center, University of California, Davis. The cultivar AC was originally obtained from the Glasshouse Crops Research Institute (Littlehampton, Sussex, UK). As the genetic background of LA2467 was not known, a segregating $BC_3F_2$ population was generated from an initial cross of LA2467 (*pe/pe*) with AC (*PE/PE*) as the recurrent parent. The mutant plants (*pe/pe*) were selected based on phenotype; short stature, pale green color of the stem and leaves, and stickiness of the fruit surface, all of which cosegregated. This population was used for all experiments. Unless otherwise stated, plants were grown in peat-based compost supplemented with fertilizer in greenhouses at Michigan State University under 16 h day (25°C) and 8 h night (20°C). Arabidopsis (*Arabidopsis thaliana*) seeds of *anl2* (SALK_000196) were described previously (Nakamura et al., 2006) and sown in soil (1:1:1 Sure mix:Medium vermiculite:Perlite, MI Grower Products Inc., www.suremix.com) and after 3 d at 4°C, maintained in a growth chamber under a 16 h photoperiod (145 $\mu$mol $m^{-2}$ $s^{-1}$) at 22°C at a relative humidity of 65%. Tomato (*Solanum lycopersicum*) fruits were harvested when they reached 35 to 40 mm diameter for green stage or at 7 d after the onset of ripening (breaker + 7 d) for ripe stage of development. All experiments involving leaves, stems, and roots were performed on 5-week-old plants unless otherwise stated. Rosette leaves from 7-week-old Arabidopsis plants were used for cutin analysis.

### Extraction and Analysis of Cuticular Lipids

Extraction of surface waxes from leaf, root, and fruit tissues of tomato or from leaves of Arabidopsis was accomplished through dipping tissue samples in chloroform containing 1% methanol for 2 min in the case of fruits and 1 min for other tissues. The surface areas of leaves and fruits were determined prior to wax extraction using a LI-3100C area meter (Li-Cor, http://www.licor.com) and Tomato Analyzer version 2.1.0.0., respectively (Brewer et al., 2006). Internal standards of tetracosane, hexadecanol and heptadecanoic acid (5 $\mu$g/mL each), and $\omega$-pentadecalactone and methyl heptadecanoate (10 $\mu$g/mL each; Sigma-Aldrich, http://www.sigmaaldrich.com) were added to each wax and cutin extract, respectively. Preparation of trimethyl-silyl derivatives of wax components, followed by delipidation, base-catalyzed transmethylation, and acetyl derivatization of cutin monomers from all the tissues was performed as previously described (Molina et al., 2006). Gas chromatography (GC)-flame ionization detector (6890N, Agilent Technologies) analysis of the derivatized wax or fatty acid methyl ester products used a DB-5 capillary column. GC temperature was programmed from 140°C to 310°C for cutin and to 330°C for wax, at 5°C $min^{-1}$. Samples were injected in split mode (330°C injector temperature). Quantification was based on flame ionization detector ion current using peak areas relative to internal standard peak areas. When necessary, compound identification was performed by GC-mass spectrometry (MS; EI mode) using an Agilent Technologies 6850 GC, equipped with an HP-5 MS column connected to an Agilent 5975 mass spectrometer. Helium was used as carrier gas at 2 mL $min^{-1}$ and oven temperature was programmed from 120°C to 340°C at 10°C $min^{-1}$. Splitless injection was used and ions were collected in scan mode (40–800 atomic mass units) with peaks quantified on the basis of their total ion current.

### Imaging of Cuticular Lipids and SEM

Cryosections of fruit pericarp, 8-$\mu$m thick, were generated using a Microm HM550 cryostat (Thermo scientific, http://www.thermoscientific.com) and stored at −20°C. Sections were stained using Sudan IV, 0.1% w/v in isopropyl alcohol. Bright-field images were collected using an Olympus IX81 inverted microscope (Olympus, www.olympus.com) configured with UPlan SApo 20× objective, NA0.75. The images were captured using an Olympus DP72 color camera and analyzed with DP2-BSW software. For imaging of fruit cuticles by SEM, fruits were hand sectioned and fixed for 30 min in 4% glutaraldehyde followed by 30 min incubation in 0.1 M phosphate buffer (pH 7.4). Further processing of samples and imaging are according to Li et al. (2007). The same procedures were followed for collecting leaf stomatal images.

### Imaging Anthocyanin Distribution

Images of hand-cut cross sections of stem tissue were collected using an Olympus FluoView FV1000 confocal laser-scanning microscope (Olympus) configured on IX81 inverted microscope with a 10× UPLSAPO objective, NA0.4. An excitation wavelength of 559 nm was generated using solid state laser, while the fluorescence emission was collected using a 570 to 640 nm band pass filter, to eliminate the detection of chlorophyll fluorescence. The differential interference contrast transmitted laser light image was collected using the 559-nm laser line and the images presented as overlays of confocal and differential interference contrast images.

### Determination of Stomatal and Trichome Densities

For stomatal density measurements, leaf surface imprints on abaxial sides of the leaf surface were taken using transparent nail polish and placed onto microscope slides. Imaging was performed using a Zeiss Axiophot microscope (Carl Zeiss, Inc., http://www.zeiss.com) at 20×, image processing was accomplished using Image-pro plus image analysis software (Media Cybernetics, http://www.mediacy.com). Stomatal density was expressed as number of stomata in five different fields of 0.55 $mm^2$ per leaflet of five individual leaflets. Trichome density was analyzed on 3-week-old plants of AC, M82, *pe*, and *cd2* using plant growth conditions and methods previously described (Kang et al., 2010).

### Analysis of Volatile Terpenes from Tomato Trichomes

Volatile terpene levels were determined in 3-week-old plants. Briefly, a leaflet from the second newly emerging leaf was dipped in 1 mL of methyl *tert*-butyl ether containing 5 ng/$\mu$L of tetradecane as an internal standard, and allowed to rock for 1 min. GC-MS analysis was performed as previously described (Schilmiller et al., 2009). Terpene identification was based on comparison of mass spectra and retention times with those available in an essential oil library (Adams, 2009).

## Determination of Fruit Glossiness

The glossiness of red-ripe fruits was measured using a custom-made gonioreflectometer consisting of a Fire-iTM digital camera (http://www.unibrain.com) and two 60-W incandescent light bulbs located in a light-impervious container. Thirty images were taken for each fruit, as it rotated 360°. The average number of saturated blue pixels for all the images was recorded as an index of fruit gloss measured in gloss units (a gloss unit is defined as number of pixels above the saturation threshold that is fixed based on specular reflectance of the sample image) programmed using MATLAB (MathWorks, www.mathworks.com). The instrument was calibrated using standard glossy and nonglossy green and red spheres prior to data collection.

## Mechanical Analysis of the Fruit Cuticle

Young's elastic modulus (Y) of isolated tomato cuticles of 3 × 0.5 cm dimension was measured using a dynamic mechanical analyzer Q800 (TA Instruments http://www.tainstruments.com) in constant stress ramp mode at room temperature until breakage was observed. Y values were calculated using Universal Analysis 2000 software (TA Instruments).

## Determination of Anthocyanin and Chlorophyll Content

Anthocyanins were extracted from leaves according to Peters et al. (1998). The absorbance ($A_{535}$) of the aqueous phase was determined spectrophotometrically using a Hitachi U3000 spectrophotometer (Hitachi High Technologies America, Inc., http://www.hitachi-hta.com). Chlorophyll content was sampled from three leaf discs. Discs were incubated in darkness for 48 h at 4°C in 100% dimethyl sulfoxide. $A_{647}$ and $A_{664}$ were determined spectrophotometrically as described above. Chlorophyll *a* and *b* were calculated according to Moran (1982).

## Determination of Leaf Epidermal Permeability

Leaf water conductance was measured using Li-Cor 6400 (Li-Cor). Plants were dark acclimated for 3 h prior to measurements being made to eliminate the effect of stomatal conductance. Chlorophyll-leaching assays were performed on fully expanded leaves. The amount of chlorophyll extracted into the solution was quantified every 30 min as described above and data were expressed as a percentage of the total chlorophyll extracted after 24 h according to Kosma et al. (2009).

## Lignin Analysis

Lignin was extracted as previously described (Foster et al., 2010). Results are reported as % ABSL based on the dry weight of the alcohol insoluble residue according to York et al. (1986), Fukushima et al. (1991), and Robinson and Mansfield (2009). For the calculation of % ABSL content of tomato, the molar extinction coefficient for Arabidopsis (23.35 $g^{-1}$ L $cm^{-1}$) was used as an estimate given that no tomato-specific coefficients were available at the time of analysis (Chang et al., 2008).

## Genetic Mapping

An interspecific F2 population of 114 individuals derived from a cross between tomato (*pe/pe*; LA2467) and *S. pimpinellifolium* (*PE/PE*; LA1589), was phenotyped for paleness of the vegetative tissues and stickiness of the fruit peel and simultaneously genotyped with chromosome 1 molecular markers, previously selected to be polymorphic between LA2467 and LA1589 (Supplemental Table S4). Genomic DNA was extracted from expanding leaves as previously described (Barry et al., 2005). Details of genetic maps and molecular markers can be accessed through the Sol Genomics Network (http://solgenomics.net).

## Cloning of *CD2* and Phylogenetic Analysis

Total RNA was extracted from expanding leaves of AC and *pe* using the RNeasy mini kit (Qiagen, http://www.qiagen.com). One microgram of RNA was used as a template for oligo dT primed first-strand cDNA synthesis using the transcriptor first-strand cDNA synthesis kit (Roche Applied Science, https://www.roche-applied-science.com). The coding region of *CD2* was amplified from cDNA using *Pfu* Ultra DNA polymerase (Agilent technologies, http://www.home.agilent.com) using the primers CD2-F and CD2-R (Supplemental Table S5). PCR fragments were purified using the PureLink PCR purification kit (Invitrogen, http://www.invitrogen.com) and cloned into the pCR4Blunt-TOPO vector (Invitrogen). Sequencing of inserts was accomplished using vector primers and the gene-specific primers CD1 through CD6 (Supplemental Table S5). Sequences were assembled using Sequencher 4.7 software (Gene Codes Corporation, http://genecodes.com). A neighbor-joining phylogenetic tree was constructed from a multiple sequence alignment of the deduced full-length amino acid sequences of selected *CD2* homologs using MEGA V5.0 software (Supplemental Table S6; Tamura et al., 2011).

## Construct Assembly and Silencing of *CD2*

Two constructs, CD2V1 and CD2V2, were assembled in the TRV2-LIC vector as previously described (Dong et al., 2007) using the primers CD2V1-F, CD2V1-R, CD2V2-F, and CD2V2-R (Supplemental Table S5). VIGS experiments were performed as described by Velasquez et al. (2009). Tomato cotyledons were infiltrated with *Agrobacterium tumefaciens* strain GV3101 cultures before the appearance of the first true leaves and tissues were harvested 4 weeks after infiltration. TRV2-LIC empty vector plants were used as controls and *TRV2::PHYTOENE DESATURASE* plants were used to monitor the progression of gene silencing. The VIGS plants were maintained in a growth chamber under a 16 h photoperiod (145 $\mu$mol $m^{-2}$ $s^{-1}$) at a constant temperature of 27°C and a relative humidity of 60%.

## Quantitative Reverse Transcription PCR Analysis

For *CD2* expression analysis stems were divided into stem peel, stem core (stem devoid of peel), and whole stem. Total RNA was isolated as described above. RNA was treated on column with DNase (Qiagen) and 1 $\mu$g of RNA was used for reverse transcription using SuperScript III first-strand synthesis system (Invitrogen). Gene-specific primers for the analyzed genes were designed by Primer Express 3.0 (ABI; listed in Supplemental Table S5). The PCR reactions were performed with FAST SYBR master mix, 2× (ABI, http://www.appliedbiosystems.com) in a 25 $\mu$L volume using an Applied Biosystems StepOnePlus real-time PCR system (ABI) with the following cycling program: 10 min at 95°C, 15 s at 95°C followed by 40 cycles of 1 min at 60°C, 15 s at 95°C, and 1 min at 60°C. The comparative ΔΔCT method was performed according to Balaji et al. (2008).

## Statistical Analyses

Statistical analyses were performed using SAS (SAS Institute, www.sas.com). The genotypic constituents were evaluated by Student's *t* test and least square means.

## Supplemental Data

The following materials are available in the online version of this article.

**Supplemental Figure S1.** Volatile terpene levels in AC and *pe*.

**Supplemental Figure S2.** Suberin and root wax composition in AC and *pe*.

**Supplemental Figure S3.** Comparison of leaf cutin and wax composition in M82 and *cd2*.

**Supplemental Figure S4.** Trichome density on leaves and anthocyanin accumulation in leaves and stem peels of M82 and *cd2*.

**Supplemental Table S1.** Lignin composition of leaves and stems in AC and *pe*.

**Supplemental Table S2.** Total wax load in fruits of AC and *pe*.

**Supplemental Table S3.** Fruit wax composition of AC and *pe*.

**Supplemental Table S4.** PCR-based genetic markers flanking the *pe* locus.

**Supplemental Table S5.** Oligonucleotide primers used in the study.

**Supplemental Table S6.** *CD2*-related genes utilized in phylogenetic analysis.

## ACKNOWLEDGMENTS

We thank Carol Flegler, and Drs. Melinda Frame and Alicia Pastor (Centre for Advanced Microscopy, Michigan State University) for assistance with

microscopy. We are grateful to Dr. Renfu Lu (Department of Biosystems and Agricultural Engineering, Michigan State University) for help with glossiness measurements; Clifton Foster and the Analytical Cell Wall Facility (Great Lakes Bio-Energy Research Center, Michigan State University) for lignin analysis; Dr. Michael Rich (Composite Materials and Structure Center, College of Engineering, Michigan State University) for guidance with dynamic mechanical analyzer experiments; and Dr. Eliana Gonzales-Vigil (Department of Horticulture, Michigan State University) for help with analysis of trichome chemistry. We also thank Dr. Jocelyn Rose (Cornell University) and Dr. Taku Takahashi (Okayama University) for providing seeds of the *cd2* allele and *anl2* mutant, respectively.

Received April 10, 2012; accepted May 18, 2012; published May 22, 2012.

## LITERATURE CITED

**Abe M, Katsumata H, Komeda Y, Takahashi T** (2003) Regulation of shoot epidermal cell differentiation by a pair of homeodomain proteins in Arabidopsis. Development **130:** 635–643

**Adams RP** (2009) Identification of Essential Oil Components by Gas Chromatography/Mass Spectrometry, Ed 4. Allured Books, Carol Stream, IL

**Aharoni A, Dixit S, Jetter R, Thoenes E, van Arkel G, Pereira A** (2004) The SHINE clade of AP2 domain transcription factors activates wax biosynthesis, alters cuticle properties, and confers drought tolerance when overexpressed in *Arabidopsis*. Plant Cell **16:** 2463–2480

**Balaji V, Mayrose M, Sherf O, Jacob-Hirsch J, Eichenlaub R, Iraki N, Manulis-Sasson S, Rechavi G, Barash I, Sessa G** (2008) Tomato transcriptional changes in response to *Clavibacter michiganensis* subsp. *michiganensis* reveal a role for ethylene in disease development. Plant Physiol **146:** 1797–1809

**Bargel H, Koch K, Cerman Z, Neinhuis C** (2006) Structure-function relationships of the plant cuticle and cuticular waxes—a smart material? Funct Plant Biol **33:** 893–910

**Bargel H, Neinhuis C** (2005) Tomato (*Lycopersicon esculentum* Mill.) fruit growth and ripening as related to the biomechanical properties of fruit skin and isolated cuticle. J Exp Bot **56:** 1049–1060

**Barry CS, McQuinn RP, Thompson AJ, Seymour GB, Grierson D, Giovannoni JJ** (2005) Ethylene insensitivity conferred by the *Green-ripe* and *Never-ripe 2* ripening mutants of tomato. Plant Physiol **138:** 267–275

**Beggs CJ, Kuhn K, Bocker R, Wellmann E** (1987) Phytochrome-induced flavonoid biosynthesis in mustard (*Sinapis alba L.*) cotyledons: enzymic control and differential regulation of anthocyanin and quercetin formation. Planta **172:** 121–126

**Bourdenx B, Bernard A, Domergue F, Pascal S, Léger A, Roby D, Pervent M, Vile D, Haslam RP, Napier JA, et al** (2011) Overexpression of Arabidopsis *ECERIFERUM1* promotes wax very-long-chain alkane biosynthesis and influences plant response to biotic and abiotic stresses. Plant Physiol **156:** 29–45

**Brewer MT, Lang LX, Fujimura K, Dujmovic N, Gray S, van der Knaap E** (2006) Development of a controlled vocabulary and software application to analyze fruit shape variation in tomato and other plant species. Plant Physiol **141:** 15–25

**Brown DE, Rashotte AM, Murphy AS, Normanly J, Tague BW, Peer WA, Taiz L, Muday GK** (2001) Flavonoids act as negative regulators of auxin transport in vivo in Arabidopsis. Plant Physiol **126:** 524–535

**Buschhaus C, Jetter R** (2011) Composition differences between epicuticular and intracuticular wax substructures: how do plants seal their epidermal surfaces? J Exp Bot **62:** 841–853

**Butler L** (1952) *Sticky peel* (*pe*) a new character in the seventh linkage group. Rep Tomato Genet Coop **2:** 2

**Chang XF, Chandra R, Berleth T, Beatson RP** (2008) Rapid, microscale, acetyl bromide-based method for high-throughput determination of lignin content in *Arabidopsis thaliana*. J Agric Food Chem **56:** 6825–6834

**Chen XB, Goodwin SM, Boroff VL, Liu XL, Jenks MA** (2003) Cloning and characterization of the *WAX2* gene of *Arabidopsis* involved in cuticle membrane and wax production. Plant Cell **15:** 1170–1185

**Christie PJ, Alfenito MR, Walbot V** (1994) Impact of low-temperature stress on general phenylpropanoid and anthocyanin pathways: enhancement of transcript abundance and anthocyanin pigmentation in maize seedlings. Planta **194:** 541–549

**Cooper-Driver GA** (2001) Biological roles for phenolic compounds in the evolution of early land plants. *In* PG Gensel, D Edwards, eds, Plants Invade the Land: Evolution and Environmental Perspectives. Columbia University Press, New York, pp 159–172

**Darby L, Ritchie D, Taylor I** (1978) Isogenic lines of the tomato "Ailsa Craig". *In* Annual Report Glasshouse Crops Research Institute, 1977, Littlehampton, UK, pp 168–184

**Dong Y, Burch-Smith TM, Liu Y, Mamillapalli P, Dinesh-Kumar SP** (2007) A ligation-independent cloning tobacco rattle virus vector for high-throughput virus-induced gene silencing identifies roles for *NbMADS4-1* and *-2* in floral development. Plant Physiol **145:** 1161–1170

**Edwards D, Abbott GD, Raven JA** (1996) Cuticles of early land plants: a palaeoecophysiological evaluation. *In* G Kerstiens, ed, Plant Cuticles: An Integrated Functional Approach. Bios Scientific Publishers, Oxford, pp 1–32

**Emmons CLW, Scott JW** (1997) Environmental and physiological effects on cuticle cracking in tomato. J Am Soc Hortic Sci **122:** 797–801

**Emmons CLW, Scott JW** (1998) Ultrastructural and anatomical factors associated with resistance to cuticle cracking in tomato (*Lycopersicon esculentum* Mill.). Int J Plant Sci **159:** 14–22

**Foster CE, Martin TM, Pauly M** (2010) Comprehensive compositional analysis of plant cell walls (Lignocellulosic biomass) part I: lignin. J Vis Exp **37:** 1745

**Fuglevand G, Jackson JA, Jenkins GI** (1996) UV-B, UV-A, and blue light signal transduction pathways interact synergistically to regulate chalcone synthase gene expression in *Arabidopsis*. Plant Cell **8:** 2347–2357

**Fukushima RS, Dehority BA, Loerch SC** (1991) Modification of a colorimetric analysis for lignin and its use in studying the inhibitory effects of lignin on forage digestion by ruminal microorganisms. J Anim Sci **69:** 295–304

**Gallego-Giraldo L, Escamilla-Trevino L, Jackson LA, Dixon RA** (2011) Salicylic acid mediates the reduced growth of lignin down-regulated plants. Proc Natl Acad Sci USA **108:** 20814–20819

**Glover BJ** (2000) Differentiation in plant epidermal cells. J Exp Bot **51:** 497–505

**Gray JE, Holroyd GH, van der Lee FM, Bahrami AR, Sijmons PC, Woodward FI, Schuch W, Hetherington AM** (2000) The HIC signalling pathway links CO2 perception to stomatal development. Nature **408:** 713–716

**Grncarevic M, Radler F** (1967) The effect of wax components on cuticular transpiration-model experiments. Planta **75:** 23–27

**Hahlbrock K, Scheel D** (1989) Physiology and molecular biology of phenylpropanoid metabolism. Annu Rev Plant Physiol Plant Mol Biol **40:** 347–369

**Hichri I, Barrieu F, Bogs J, Kappel C, Delrot S, Lauvergeat V** (2011) Recent advances in the transcriptional regulation of the flavonoid biosynthetic pathway. J Exp Bot **62:** 2465–2483

**Hovav R, Chehanovsky N, Moy M, Jetter R, Schaffer AA** (2007) The identification of a gene (*Cwp1*), silenced during *Solanum* evolution, which causes cuticle microfissuring and dehydration when expressed in tomato fruit. Plant J **52:** 627–639

**Ingram G** (2008) Epidermal signalling and the control of plant shoot growth. *In* L Bogre, G Beemster, eds, Plant Growth Signaling, Vol 10. Springer, Berlin, pp 127–153

**Ingram GC, Boisnard-Lorig C, Dumas C, Rogowsky PM** (2000) Expression patterns of genes encoding HD-ZipIV homeo domain proteins define specific domains in maize embryos and meristems. Plant J **22:** 401–414

**Ingram GC, Magnard JL, Vergne P, Dumas C, Rogowsky PM** (1999) *ZmOCL1*, an *HDGL2* family homeobox gene, is expressed in the outer cell layer throughout maize development. Plant Mol Biol **40:** 343–354

**Isaacson T, Kosma DK, Matas AJ, Buda GJ, He YH, Yu BW, Pravitasari A, Batteas JD, Stark RE, Jenks MA, et al** (2009) Cutin deficiency in the tomato fruit cuticle consistently affects resistance to microbial infection and biomechanical properties, but not transpirational water loss. Plant J **60:** 363–377

**Javelle M, Klein-Cosson C, Vernoud V, Boltz V, Maher C, Timmermans M, Depège-Fargeix N, Rogowsky PM** (2011a) Genome-wide characterization of the HD-ZIP IV transcription factor family in maize: preferential expression in the epidermis. Plant Physiol **157:** 790–803

**Javelle M, Vernoud V, Depège-Fargeix N, Arnould C, Oursel D, Domergue F, Sarda X, Rogowsky PM** (2010) Overexpression of the epidermis-specific homeodomain-leucine zipper IV transcription factor Outer Cell Layer1 in maize identifies target genes involved in lipid metabolism and cuticle biosynthesis. Plant Physiol **154:** 273–286

**Javelle M, Vernoud V, Rogowsky PM, Ingram GC** (2011b) Epidermis: the formation and functions of a fundamental plant tissue. New Phytol **189:** 17–39

**Kang JH, Shi F, Jones AD, Marks MD, Howe GA** (2010) Distortion of trichome morphology by the hairless mutation of tomato affects leaf surface chemistry. J Exp Bot **61:** 1053–1064

**Kolattukudy PE** (1980) Biopolyester membranes of plants: cutin and suberin. Science **208:** 990–1000

**Kosma DK, Bourdenx B, Bernard A, Parsons EP, Lü S, Joubès J, Jenks MA** (2009) The impact of water deficiency on leaf cuticle lipids of Arabidopsis. Plant Physiol **151:** 1918–1929

**Kubo H, Kishi M, Goto K** (2008) Expression analysis of *ANTHOCYANINLESS2* gene in Arabidopsis. Plant Sci **175:** 853–857

**Kubo H, Peeters AJ, Aarts MG, Pereira A, Koornneef M** (1999) *ANTHOCYANINLESS2*, a homeobox gene affecting anthocyanin distribution and root development in *Arabidopsis*. Plant Cell **11:** 1217–1226

**Kurata T, Kawabata-Awai C, Sakuradani E, Shimizu S, Okada K, Wada T** (2003) The YORE-YORE gene regulates multiple aspects of epidermal cell differentiation in Arabidopsis. Plant J **36:** 55–66

**Landry LG, Chapple CC, Last RL** (1995) Arabidopsis mutants lacking phenolic sunscreens exhibit enhanced ultraviolet-B injury and oxidative damage. Plant Physiol **109:** 1159–1166

**Leide J, Hildebrandt U, Reussing K, Riederer M, Vogg G** (2007) The developmental pattern of tomato fruit wax accumulation and its impact on cuticular transpiration barrier properties: effects of a deficiency in a *beta-ketoacyl-coenzyme A synthase* (*LeCER6*). Plant Physiol **144:** 1667–1679

**Li H, Pinot F, Sauveplane V, Werck-Reichhart D, Diehl P, Schreiber L, Franke R, Zhang P, Chen L, Gao YW, et al** (2010a) Cytochrome P450 family member *CYP704B2* catalyzes the omega-hydroxylation of fatty acids and is required for anther cutin biosynthesis and pollen exine formation in rice. Plant Cell **22:** 173–190

**Li JY, Ou-Lee TM, Raba R, Amundson RG, Last RL** (1993) *Arabidopsis* flavonoid mutants are hypersensitive to UV-B irradiations. Plant Cell **5:** 171–179

**Li X, Bonawitz ND, Weng J-K, Chapple C** (2010b) The growth reduction associated with repressed lignin biosynthesis in *Arabidopsis thaliana* is independent of flavonoids. Plant Cell **22:** 1620–1632

**Li YH, Beisson F, Koo AJK, Molina I, Pollard M, Ohlrogge J** (2007) Identification of acyltransferases required for cutin biosynthesis and production of cutin with suberin-like monomers. Proc Natl Acad Sci USA **104:** 18339–18344

**Li-Beisson Y, Pollard M, Sauveplane V, Pinot F, Ohlrogge J, Beisson F** (2009) Nanoridges that characterize the surface morphology of flowers require the synthesis of cutin polyester. Proc Natl Acad Sci USA **106:** 22008–22013

**Li-Beisson Y, Shorrosh B, Beisson F, Andersson MX, Arondel V, Bates PD, Baud Sb, Bird D, DeBono A, Durrett TP, et al** (2010) Acyl-lipid metabolism. *In* R Last, ed, The Arabidopsis Book, Vol 8. The American Society of Plant Biologists, Rockville, MD, pp 1–65

**Lu P, Porat R, Nadeau JA, O'Neill SD** (1996) Identification of a meristem L1 layer-specific gene in *Arabidopsis* that is expressed during embryonic pattern formation and defines a new class of homeobox genes. Plant Cell **8:** 2155–2168

**Martin C, Gerats T** (1993) Control of pigment biosynthesis genes during petal development. Plant Cell **5:** 1253–1264

**Matas AJ, Cobb ED, Bartsch JA, Paolillo DJ Jr, Niklas KJ** (2004) Biomechanics and anatomy of *Lycopersicon esculentum* fruit peels and enzyme-treated samples. Am J Bot **91:** 352–360

**Matas AJ, Yeats TH, Buda GJ, Zheng Y, Chatterjee S, Tohge T, Ponnala L, Adato A, Aharoni A, Stark R, et al** (2011) Tissue- and cell-type specific transcriptome profiling of expanding tomato fruit provides insights into metabolic and regulatory specialization and cuticle formation. Plant Cell **23:** 3893–3910

**McFarlane HE, Shin JJH, Bird DA, Samuels AL** (2010) *Arabidopsis* ABCG transporters, which are required for export of diverse cuticular lipids, dimerize in different combinations. Plant Cell **22:** 3066–3075

**Mintz-Oron S, Mandel T, Rogachev I, Feldberg L, Lotan O, Yativ M, Wang Z, Jetter R, Venger I, Adato A, et al** (2008) Gene expression and metabolism in tomato fruit surface tissues. Plant Physiol **147:** 823–851

**Molina I, Bonaventure G, Ohlrogge J, Pollard M** (2006) The lipid polyester composition of *Arabidopsis thaliana* and *Brassica napus* seeds. Phytochemistry **67:** 2597–2610

**Moran R** (1982) Formulae for determination of chlorophyllous pigments extracted with n,n-dimethylformamide. Plant Physiol **69:** 1376–1381

**Mukherjee K, Brocchieri L, Bürglin TR** (2009) A comprehensive classification and evolutionary analysis of plant homeobox genes. Mol Biol Evol **26:** 2775–2794

**Mutschler MA, Tanksley SD, Rick CM** (1987) Linkage maps of the tomato. Rep Tomato Genet Coop **37:** 5–28

**Nakamura M, Katsumata H, Abe M, Yabe N, Komeda Y, Yamamoto KT, Takahashi T** (2006) Characterization of the class IV homeodomain-leucine zipper gene family in Arabidopsis. Plant Physiol **141:** 1363–1375

**Panikashvili D, Savaldi-Goldstein S, Mandel T, Yifhar T, Franke RB, Höfer R, Schreiber L, Chory J, Aharoni A** (2007) The Arabidopsis *DESPERADO/AtWBC11* transporter is required for cutin and wax secretion. Plant Physiol **145:** 1345–1360

**Panikashvili D, Shi JX, Schreiber L, Aharoni A** (2009) The Arabidopsis *DCR* encoding a soluble BAHD acyltransferase is required for cutin polyester formation and seed hydration properties. Plant Physiol **151:** 1773–1789

**Peters JL, Szell M, Kendrick RE** (1998) The expression of light-regulated genes in the high-pigment-1 mutant of tomato. Plant Physiol **117:** 797–807

**Pollard M, Beisson F, Li YH, Ohlrogge JB** (2008) Building lipid barriers: biosynthesis of cutin and suberin. Trends Plant Sci **13:** 236–246

**Ponting CP, Aravind L** (1999) START: a lipid-binding domain in StAR, HD-ZIP and signalling proteins. Trends Biochem Sci **24:** 130–132

**Qin B-X, Tang D, Huang J, Li M, Wu X-R, Lu L-L, Wang K-J, Yu H-X, Chen J-M, Gu M-H, et al** (2011) Rice *OsGL1-1* is involved in leaf cuticular wax and cuticle membrane. Mol Plant **4:** 985–995

**Riederer M, Schreiber L** (2001) Protecting against water loss: analysis of the barrier properties of plant cuticles. J Exp Bot **52:** 2023–2032

**Robinson AR, Mansfield SD** (2009) Rapid analysis of poplar lignin monomer composition by a streamlined thioacidolysis procedure and near-infrared reflectance-based prediction modeling. Plant J **58:** 706–714

**Samuels L, Kunst L, Jetter R** (2008) Sealing plant surfaces: cuticular wax formation by epidermal cells. Annu Rev Plant Biol **59:** 683–707

**Schilmiller AL, Last RL, Pichersky E** (2008) Harnessing plant trichome biochemistry for the production of useful compounds. Plant J **54:** 702–711

**Schilmiller AL, Schauvinhold I, Larson M, Xu R, Charbonneau AL, Schmidt A, Wilkerson C, Last RL, Pichersky E** (2009) Monoterpenes in the glandular trichomes of tomato are synthesized from a neryl diphosphate precursor rather than geranyl diphosphate. Proc Natl Acad Sci USA **106:** 10865–10870

**Schreiber L** (2010) Transport barriers made of cutin, suberin and associated waxes. Trends Plant Sci **15:** 546–553

**Seo PJ, Lee SB, Suh MC, Park MJ, Go YS, Park CM** (2011) The MYB96 transcription factor regulates cuticular wax biosynthesis under drought conditions in *Arabidopsis*. Plant Cell **23:** 1138–1152

**Sieber P, Schorderet M, Ryser U, Buchala A, Kolattukudy P, Métraux J-P, Nawrath C** (2000) Transgenic *Arabidopsis* plants expressing a fungal cutinase show alterations in the structure and properties of the cuticle and postgenital organ fusions. Plant Cell **12:** 721–738

**Steyn WJ, Wand SJE, Holcroft DM, Jacobs G** (2002) Anthocyanins in vegetative tissues: a proposed unified function in photoprotection. New Phytol **155:** 349–361

**Suh MC, Samuels AL, Jetter R, Kunst L, Pollard M, Ohlrogge J, Beisson F** (2005) Cuticular lipid composition, surface structure, and gene expression in Arabidopsis stem epidermis. Plant Physiol **139:** 1649–1665

**Tamura K, Peterson D, Peterson N, Stecher G, Nei M, Kumar S** (2011) MEGA5: molecular evolutionary genetics analysis using maximum likelihood, evolutionary distance, and maximum parsimony methods. Mol Biol Evol **28:** 2731–2739

**Velasquez AC, Chakravarthy S, Martin GB** (2009) Virus-induced gene silencing (VIGS) in Nicotiana benthamiana and tomato. J Vis Exp **10:** 1292

**Vogg G, Fischer S, Leide J, Emmanuel E, Jetter R, Levy AA, Riederer M** (2004) Tomato fruit cuticular waxes and their effects on transpiration barrier properties: functional characterization of a mutant deficient in a very-long-chain fatty acid beta-ketoacyl-CoA synthase. J Exp Bot **55:** 1401–1410

**Vogt T** (2010) Phenylpropanoid biosynthesis. Mol Plant **3:** 2–20

**Wang ZY, Xiong LM, Li WB, Zhu JK, Zhu JH** (2011) The plant cuticle is required for osmotic stress regulation of abscisic acid biosynthesis and osmotic stress tolerance in *Arabidopsis*. Plant Cell **23:** 1971–1984

**Wu R, Li S, He S, Wassmann F, Yu C, Qin G, Schreiber L, Qu L-J, Gu H** (2011) CFL1, a WW domain protein, regulates cuticle development by modulating the function of *HDG1*, a class IV homeodomain transcription factor, in rice and *Arabidopsis*. Plant Cell **23:** 3392–3411

**Yang J, Isabel Ordiz M, Jaworski JG, Beachy RN** (2011) Induced accumulation of cuticular waxes enhances drought tolerance in Arabidopsis by changes in development of stomata. Plant Physiol Biochem **49:** 1448–1455

**Yeats TH, Howe KJ, Matas AJ, Buda GJ, Thannhauser TW, Rose JKC** (2010) Mining the surface proteome of tomato (*Solanum lycopersicum*) fruit for proteins associated with cuticle biogenesis. J Exp Bot **61:** 3759–3771

**York WS, Darvill AG, McNeil M, Stevenson TT, Albersheim P, Arthur Weissbach HW** (1986) Isolation and characterization of plant cell walls and cell wall components. Methods Enzymol **118:** 3–40